Chapter 6 Introduction to Planetary Boundary Layer

Yuh-Lang Lin
Dynamic Meteorology (EES751)
Department of Energy & Environmental Systems
North Carolina A&T State University
http://mesolab.ncat.edu

6.1 Introduction

- Planetary boundary layer (PBL) has 2 effects: (1) friction and (2) heat flux.

- There are several sublayers of the PBL, namely *surface layer*, *mixed layer*, transition layer, and *free atmosphere*.

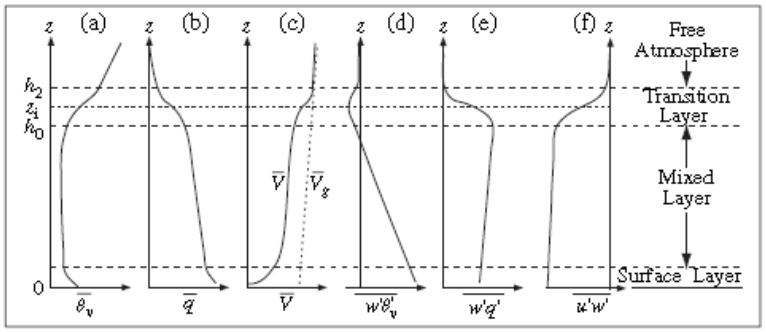

Fig. 14.2 Typical convective boundary layer profiles of (a) mean virtual potential temperature, (b) specific humidity, (c) wind speed ($\overline{V}$ and $\overline{V}_g$ denote mean wind speed and geostrophic wind speed respectively), (d) vertical heat flux, (e) vertical moisture flux, and (f) vertical momentum flux. (Adapted after Driedonks and Tennekes 1984.)

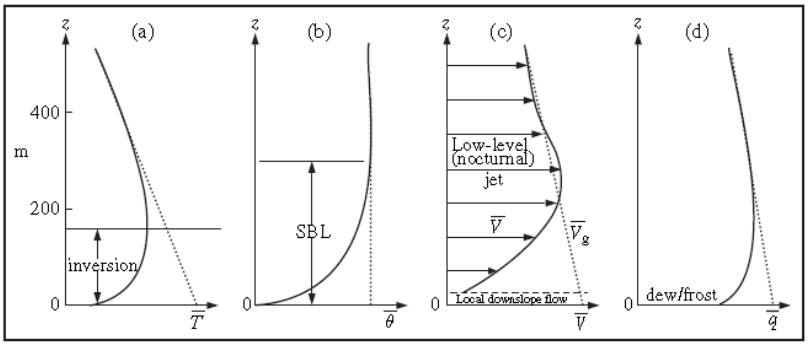

Fig. 14.3 Typical stable boundary layer (SBL) profiles of (a) mean temperature, (b) potential temperature, (c) wind speed, and (d) specific humidity. (Adapted after Stull 1988, with kind permission of Springer Sciences and Media.)

6.2 Reynolds Averaging and Closure Problem

Following the scheme originally developed by Reynolds (1895), each variable of the governing equations is decomposed into a slow-varying mean field and a rapid-varying turbulent part,

$$u = \bar{u} + u',\ v = \bar{v} + v',\ w = \bar{w} + w',\ \theta = \bar{\theta} + \theta',$$

$$p = \bar{p} + p', \text{ and } \rho = \bar{\rho} + \rho'.$$

The fully compressible fluid system may be written as (e.g., Lin 2007)

$$\frac{Du}{Dt} = fv - \frac{1}{\rho}\frac{\partial p}{\partial x} + \nu\nabla^2 u, \tag{13.5.6}$$

$$\frac{Dv}{Dt} = -fu - \frac{1}{\rho}\frac{\partial p}{\partial y} + \nu\nabla^2 v, \tag{13.5.7}$$

$$\frac{Dw}{Dt} = -\frac{1}{\rho}\frac{\partial p}{\partial z} - g + \nu\nabla^2 w, \tag{13.5.8}$$

$$\frac{D\theta_v}{Dt} = S_\theta + \kappa\nabla^2\theta \tag{13.5.9}$$

$$\frac{D\phi}{Dt} = S_\phi + \kappa\nabla^2\phi, \quad \phi = q_v, q_c\ ,\ q_i,\ q_r,\ q_s,\ q_g\ , \tag{13.5.10}$$

$$\frac{D\rho}{Dt} + \rho\nabla\cdot\boldsymbol{V} = 0, \tag{13.5.11}$$

$$p = \rho RT \tag{13.5.12}$$

$$\theta_v = T_v\left(\frac{p_o}{p}\right)^{R_d/c_p}, \tag{13.5.13}$$

$$T_v = T(1+0.61q_v)\,, \tag{13.5.14}$$

where

T_v is called *virtual temperature*

θ_v is the *virtual potential temperature*

p_o is the basic state pressure at the ground, usually taken as 1000 *hPa*

S_θ is any source or sink of θ_v, such as surface long-wave radiation and elevated latent heating

S_ϕ is any source or sink of the hydrometeor ϕ, such as mixing ratios of *water vapor* (q_v), *cloud water* (q_c) , *rain* (q_r), *cloud ice* (q_i), *snow* (q_s), and *graupel/hail* (q_g).

The virtual (potential) temperature is the (potential) temperature that a dry air parcel would have if its pressure and density were equal to those of a given sample of moist air. The virtual temperature is a fictitious temperature of a moist air parcel that satisfies the equation of state for dry air. More realistic and sophisticated parameterizations of planetary boundary layer processes can be adopted.

Substituting *u, v, w, θ, p* and ρ into the system of (13.5.6) – (13.5.14) leads to

$$\frac{\overline{D}\overline{u}}{Dt} = f\overline{v} - \frac{1}{\rho_o}\frac{\partial\overline{p}}{\partial x} - \frac{1}{\rho_o}\left[\frac{\partial\left(\rho_o\overline{u'u'}\right)}{\partial x} + \frac{\partial\left(\rho_o\overline{u'v'}\right)}{\partial y} + \frac{\partial\left(\rho_o\overline{u'w'}\right)}{\partial z}\right] + \nu\nabla^2\overline{u}, \tag{14.1.3}$$

$$\frac{\overline{D}\overline{v}}{Dt} = -f\overline{u} - \frac{1}{\rho_o}\frac{\partial \overline{p}}{\partial y} - \frac{1}{\rho_o}\left[\frac{\partial\left(\rho_o \overline{u'v'}\right)}{\partial x} + \frac{\partial\left(\rho_o \overline{v'v'}\right)}{\partial y} + \frac{\partial\left(\rho_o \overline{v'w'}\right)}{\partial z}\right] + \nu\nabla^2\overline{v}, \qquad (14.1.4)$$

$$\frac{\overline{D}\overline{w}}{Dt} = -\frac{1}{\rho_o}\frac{\partial p_1}{\partial z} - g\frac{\rho_1}{\rho_o} - \frac{1}{\rho_o}\left[\frac{\partial\left(\rho_o \overline{u'w'}\right)}{\partial x} + \frac{\partial\left(\rho_o \overline{v'w'}\right)}{\partial y} + \frac{\partial\left(\rho_o \overline{w'w'}\right)}{\partial z}\right] + \nu\nabla^2\overline{w}, \qquad (14.1.5)$$

$$\frac{\overline{D}\overline{\theta}_v}{Dt} = \overline{S}_\theta - \frac{1}{\rho_o}\left[\frac{\partial\left(\rho_o \overline{u'\theta'}\right)}{\partial x} + \frac{\partial\left(\rho_o \overline{v'\theta'}\right)}{\partial y} + \frac{\partial\left(\rho_o \overline{w'\theta'}\right)}{\partial z}\right] + \kappa\nabla^2\overline{\theta}, \qquad (14.1.6)$$

$$\frac{\overline{D}\overline{\phi}}{Dt} = \overline{S}_\phi - \frac{1}{\rho_o}\left[\frac{\partial\left(\rho_o \overline{u'\phi'}\right)}{\partial x} + \frac{\partial\left(\rho_o \overline{v'\phi'}\right)}{\partial y} + \frac{\partial\left(\rho_o \overline{w'\phi'}\right)}{\partial z}\right] + \kappa\nabla^2\overline{\phi},$$

$$\phi = q_v,\ q_c,\ q_i,\ q_r,\ q_s, \text{ and } q_g, \qquad (14.1.7)$$

$$\nabla\cdot\left(\rho_o\overline{\boldsymbol{V}}\right) = 0, \quad \overline{\boldsymbol{V}} = (\overline{u}, \overline{v}, \overline{w}), \qquad (14.1.8)$$

$$\overline{p} = \overline{\rho} R \overline{T}, \qquad (14.1.9)$$

$$\overline{\theta}_v = \overline{T}_v\left(\frac{p_s}{\overline{p}}\right)^{R_d/c_p}, \qquad (14.1.10)$$

$$\overline{T_v} = \overline{T}(1 + 0.61\overline{q}_v), \qquad (14.1.11)$$

$$\overline{p} = p_o + p_1;\ \overline{\rho} = \rho_o + \rho_1;\ \frac{\partial p_o}{\partial z} = -\rho_o g;\ \overline{\phi} = \phi_o + \phi_1, \qquad (14.1.12)$$

where p_s is 1000 hPa, and

$$\frac{\overline{D}}{Dt} = \frac{\partial}{\partial t} + \overline{u}\frac{\partial}{\partial x} + \overline{v}\frac{\partial}{\partial y} + \overline{w}\frac{\partial}{\partial z}, \qquad (14.1.13)$$

$$\phi_o \equiv \frac{1}{XY}\int_{-Y/2}^{Y/2}\int_{-X/2}^{X/2}\overline{\phi}\, dx\, dy. \qquad (14.1.14)$$

In the derivation, we have applied the Reynolds averaging,

$$\overline{u+w}=\bar{u}+\bar{w};\ \overline{cw}=c\bar{w};\quad \bar{\bar{w}}=\bar{w};\ \overline{w'}=0;$$

$$\overline{w'\bar{\theta}}=\overline{w'}\,\bar{\theta}=0;\ \overline{w\theta}=\overline{(\bar{w}+w')(\bar{\theta}+\theta')}=\bar{w}\,\bar{\theta}+\overline{w'\theta'}\ ;\ \overline{uw}=\bar{u}\,\bar{w}+\overline{u'w'};$$

$$\overline{\frac{\partial w}{\partial s}}=\frac{\partial \bar{w}}{\partial s};\ \overline{\frac{\partial \bar{w}}{\partial s}}=\frac{\partial \bar{w}}{\partial s};\ \int \overline{w\,ds}=\int \bar{w}\,ds;\quad s=x,y,z,\text{or}\ t, \tag{14.1.1}$$

In the above equations, the terms with ν are due to *molecular viscosity*.

Note that molecular viscosity is caused by the molecular motion which is important only in a very thin layer, i.e. the *viscous sublayer*. The viscous sublayer has a depth of O(cm). Above the viscous sublayer, the viscosity comes from the turbulent eddy motion, i.e. the *eddy viscosity*.

- Note that the equation set (14.1.3)-(14.1.11) is not a closed system mathematically since in addition to the unknown mean variables, other flux terms are also present.

- In order to make the equation set closed, we need to represent or parameterize the turbulent flux terms and the source and sink terms using the mean variables.

  The need for parameterizations poses a *closure problem*, which is a challenging task in parameterizing the PBL processes, as well as for moist and radiative transfer processes.

  The horizontal derivatives of the turbulent flux terms are normally associated with some horizontal inhomogeneities, such as cities and coastlines, which may be neglected over horizontally homogeneous regions.

- ## Direct Numerical Simulation (DNS)

D*irect numerical simulation* (*DNS*) has been developed to numerically simulate turbulent motions by fluid dynamicists, in which the time-dependent Navier-Stokes equations with explicit terms for molecular diffusion are integrated numerically to obtain the solution, without making any turbulence parameterizations. The finest scales of the simulation are determined by the balance between nonlinear advection and viscous diffusion, i.e. the *Reynolds number* (*Re = UL/ν,* where *U* and *L* are the characteristic velocity and length scales, respectively, and ν the kinematic viscosity coefficient) of the flow.

A typical value of kinematic viscosity for the air in the lower atmosphere is $1.5 \text{x} 10^{-5} m^2 s^{-1}$. When Re>>1, changes in motion by advection are much more important than the dissipation due to molecular viscosity. In this type of turbulent flow, a *turbulent Reynolds number* is more appropriately used to describe the characteristic of the flow, in which the kinematic viscosity coefficient is replaced by the *turbulent exchange coefficient*. Boundary layers encountered in engineering practice have a fairly large Reynolds numbers ranging from 10^3 to10^6, while the atmospheric boundary layers developing over most natural surfaces are characterized by even larger Reynolds numbers (10^6 to10^9). The higher Reynolds number flows have also been observed in the free atmosphere, such as within cumulus cloud and in wave breaking regions.

DNS requires the whole range of spatial and temporal scales of the turbulence to be resolved by the grid interval (Δx), from the smallest dissipative scale (L_ε), where L_ε is approximately equal to $(\nu^3/\varepsilon)^{1/4}$ and ε is the kinetic energy dissipation. To satisfy these conditions, the number of grid intervals *N* in the grid direction must satisfy $N\Delta x > L$ and $\Delta x < L_\varepsilon$, where *L* is the integral scale. Since $\varepsilon \approx U^3/L$, a three-dimensional DNS will require a number of grid intervals $N^3 \geq Re^{9/4}$. Thus, the computational cost for DNS is extremely high. With current computing power, it is unrealistic to apply DNS to mesoscale atmospheric modeling. On the other hand, even when the needed computing power is available; we still have to be careful in using the detailed information about small-scale turbulent motions and processes with sizes that cannot be resolved by available observational systems. Since these processes are not well understood at the present time, the governing equations of fluid motion cannot describe them accurately.

- ## Reynolds-averaged Navier-Stokes numerical simulation (RANS)

The second approach is to numerically integrate the Reynolds-averaged Navier-Stokes (*RANS*) equations of the mean motion. The ensemble properties of all time fluctuations in a turbulent flow are described by a turbulence closure. In this approach, the subgrid-scale motions and processes are parameterized. The parameterization approach gives a less detailed representation than the explicit representation (DNS), but it is more practical in terms of computing cost and may be sufficiently accurate for many mesoscale models since it considers grid interval and initial data, among other factors.

- ## Large-Eddy Simulation (LES)

A third approach in numerically simulating turbulent flows is to simulate *large turbulent eddies* explicitly, while the unresolved subgrid scale motions associated with smaller turbulent eddies are either ignored or parameterized. In this type of *large-eddy simulations* (*LES*), the large turbulent eddies explicitly simulated by the numerical model fall in the range of the grid size to the domain size of the model. Although the LES of turbulent flows and neutral and unstable *planetary boundary layer* (PBL) flows have been demonstrated to be very encouraging, the simulations of the nocturnal boundary layer are less successful due to the fact that the characteristic large-eddy scale becomes too small, and that most of the energy transfer and other exchange processes are overly influenced or dominated by subgrid scale motions. Although the LES derive their credibility from the explicit resolution of large-scale turbulent eddies, they depend upon a small-scale *turbulence closure* and must, to some degree, inherit the many uncertainties associated with turbulence closure (Mason 1994). Most LES results obtained so far are very encouraging, however, there is still room for improvements to overcome certain limiations. Some improvements include (a) the quality of the simulation can depend sensitively on subgrid modeling, which is not fully developed; and (b) LES requires high numerical accuracy, and does not in particular tolerate numerical dissipation which is often adopted in mesoscale models. To take advantage of both the LES and RANS, a hybrid LES-RANS approach has been developed and applied, in particular, to engineering problems.

6.3 PBL Parameterizations

a. Bulk aerodynamic parameterization

The *bulk aerodynamic parameterization* treats the boundary layer as a single slab and assumes the wind speed and potential temperature are independent of height, and the turbulence is horizontally homogeneous.

Based on these assumptions, the horizontal turbulence flux divergence terms in (14.1.3)-(14.1.7) can be neglected, and the vertical subgrid turbulence fluxes are parameterized by

$$\overline{u'w'} = -C_d \overline{V}^2 \cos\mu;\ \overline{v'w'} = -C_d \overline{V}^2 \sin\mu;\ \overline{w'\theta'} = -C_h \overline{V}\left(\overline{\theta} - \overline{\theta}_{z_o}\right), \qquad (14.2.15)$$

where C_d and C_h are nondimensional *drag* and *heat transfer coefficients*, respectively, $\overline{V} = (\overline{u}^2 + \overline{v}^2)^{1/2}$, $\mu = \tan^{-1}(\overline{v}/\overline{u})$, and z_o is the roughness or top of the surface layer. The values of $\overline{V}$, $\overline{u}$, $\overline{v}$, and $\overline{\theta}$ are evaluated at the standard anemometer height, 10 m. The bulk aerodynamic parameterization has been adopted in some GCM and regional climate models.

For a given reference height, C_d increases with increasing roughness, which ranges from 1.3×10^{-3} over ocean surface to 7×10^{-3} over rough land surface. From the formulas proposed in the parameterization of the surface layer, the expressions of C_d and C_h may be derived

$$C_d = k^2 / \left(\ln(z/z_o) - \varphi_m(z/L)\right)^2;$$
$$C_h = \beta k^2 / \left(\ln(z/z_o) - \varphi_m(z/L)\right)\left(\ln(z/z_o) - \varphi_h(z/L)\right), \qquad (14.2.16)$$

where φ_m and φ_h are defined in (14.2.8) and (14.2.12), respectively, and β is an empirical value defined in (14.2.9). As mentioned earlier, an empirical value 1.35 has been proposed for β.

Due to the assumption of height-independent wind speed and potential temperature and horizontally homogeneous turbulence, the bulk aerodynamic parameterization is more suitable for representing a well-mixed boundary layer than the neutral and stable boundary layers. Based on these assumptions, further assuming a three-way balance among the Coriolis force, pressure gradient force, and the vertical gradient of the turbulent momentum flux from (14.1.3) and (14.1.4), and using the bulk parameterization, one may derive the following equations for $\bar{u}$ and $\bar{v}$,

$$\bar{u} = \bar{u}_g - \kappa_s \overline{V}\bar{v}\,; \quad \bar{v} = \kappa_s \overline{V}\bar{u}\,, \tag{14.2.17}$$

where $\kappa_s \equiv C_d/(fh)$, h is the mixed layer height, and $\bar{u}_g$ is the geostrophic wind speed at the bottom of the mixed layer. Equation (14.2.17) can also be rewritten as

$$f\mathbf{k} \times \overline{\mathbf{V}} = -\frac{1}{\rho_o}\nabla\bar{p} - \frac{C_d}{h}\overline{V}\overline{\mathbf{V}}; \quad \overline{\mathbf{V}} = (\bar{u}, \bar{v}), \tag{14.2.18}$$

which gives a three-way balance with the wind deflected toward the low pressure. In addition, the cross-isobar flow increases as the turbulent drag increases. Note that in a rotational frame of reference or in the presence of directional shear, the frictional force on a fluid element need not be parallel and opposite to the velocity vector (e.g., Fig. 6.4 of Arya 2001), as commonly depicted in

many textbook schematics of the force balance in the frictional layer (e.g., Holton 2004).

b. K-theory parameterization

Although the bulk parameterization is simple and easy to implement in a numerical model, it cannot properly represent a neutrally and stably stratified boundary layer. The reason for this is that the wind speed and direction in this situation does vary significantly with height and the boundary layer above the surface cannot be treated as a single slab. In order to close the mathematical problem, the subgrid turbulent flux terms are assumed to be proportional to their corresponding local gradients of the mean values, analogous to molecular diffusion.

In this approach, the turbulent flux terms in (14.1.3)-(14.1.7) are written as (14.2.1).

$$\overline{u'w'} = -K_m \frac{\partial \bar{u}}{\partial z}; \quad \overline{v'w'} = -K_m \frac{\partial \bar{v}}{\partial z}; \quad \overline{w'\theta'} = -K_h \frac{\partial \bar{\theta}}{\partial z}; \quad \overline{w'q'} = -K_q \frac{\partial \bar{q}}{\partial z}, \qquad (14.2.1)$$

Similar to the bulk parameterization, the subgrid turbulent flux divergence terms are neglected. The simplest way to determine the exchange coefficients in the boundary layer is based on the *mixing length hypothesis*. Analogous to the mean free path of molecules, the mixing length hypothesis assumes that an air parcel that is displaced vertically will carry the mean properties of its original level for a characteristic length, i.e. the *mixing length* (l), before

mixing with its environment. Since $lu' \approx \partial \bar{u} / \partial z$ and K_m are proportional to lu', based on dimensional argument, we then have

$$K_m = l^2 \, \partial \bar{u} / \partial z \, . \qquad (14.2.19)$$

The eddy and thermal diffusivity coefficients, K_m and K_h, respectively, are often taken as either constants or empirically related to height and stability as calculated from NWP model output. As mentioned in the parameterization of the surface layer discussion, this approach of the parameterization of momentum, heat, and moisture fluxes is referred to as *K theory*.

The K theory is a *first-order closure* because the fluxes are parameterized proportional to the mean values. If the exchange coefficients are taken as constants, then they are referred to as *local exchange coefficients*. For example, the local exchange coefficient may be expressed as (Blackadar 1979)

Stably stratified ($\partial \bar{\theta} / \partial z > 0$):

$$K_m = K_h = 1.1(Ri_C - Ri) l^2 (\partial \bar{V} / \partial z) / Ri_C \, , \quad Ri \le Ri_C \qquad (14.2.20a)$$
$$= 0 \, , \qquad\qquad Ri > Ri_C \, ,$$

Unstably stratified ($\partial \bar{\theta} / \partial z \le 0$):

$$K_m = l^2 (\partial \bar{V} / \partial z)(1 - 21Ri)^{1/2} ; \; K_h = l^2 (\partial \bar{V} / \partial z)(1 - 87Ri)^{1/2} , \qquad (14.2.20b)$$

where $Ri_C = 0.25$ is the critical Richardson number. Note that Ri_C distinguishes whether the flow is dynamically (shear) stable or not. A value of $l = kz$ for z < 200 m (with $k = 0.35$) and 700 m for $z \ge 200$ m in (14.2.20a) has been suggested (McNider and Pielke 1981).

The *local K-theory* approach has been adopted in a number of mesoscale models as an option. In addition to Blackadar's formulation, other formulations of local exchange coefficients have also been proposed. However, approaches such as the local K-theory scheme have been found to have some deficiencies. The most serious problem in this formulation is that the transport of mass and momentum in the PBL is mostly accomplished by the largest eddies and such eddies should be parameterized by the bulk properties of the PBL instead of the local properties (e.g., Wyngaard and Brost 1984; Holtslag and Moeng 1991). The discrepancy in eddy size makes the local K-theory problematic for unstable conditions, and its implementation could induce the appearance of countergradient fluxes.

In order to resolve this problem, *non-local K-theory* has been proposed (e.g., Deardorff 1972; Troen and Mahrt 1986; Holtslag and Moeng 1991). For example, the turbulence diffusion equations for prognostic variables can be expressed by

$$\frac{\partial \phi}{\partial t} = \frac{\partial}{\partial z}\left[K_c \left(\frac{\partial \phi}{\partial z} - \gamma_C \right) \right], \qquad \phi = u,\ v,\ w,\ \theta, \text{or } q \tag{14.2.21}$$

where $K_c = K_m$ or K_h and γ_C is a correction to the local gradient that incorporates the contribution of the large-scale eddies to the total flux. The eddy diffusivity coefficient can be formulated as

$$K_m = k w_s z \left(1 - \frac{z}{h} \right)^p, \tag{14.2.22}$$

where p is the profile shape exponent taken to be 2, k is the von Karman constant (= 0.4), z is the height from the surface, h is the height of PBL, and w_s is a mixed-layer velocity scale (e.g., Troen and Mahrt 1986; Hong and Pan 1996).

Assuming a three-way balance among the Coriolis force, pressure gradient force, and the vertical gradient of the turbulent momentum flux from (14.1.3) and (14.1.4), in addition to the use of the K-theory parameterization with constant K_m, one may derive the following *Ekman layer* relationships

$$K_m \frac{\partial^2 \bar{u}}{\partial z^2} + f(\bar{v} - \bar{v}_g) = 0, \tag{14.2.23}$$

$$K_m \frac{\partial^2 \bar{v}}{\partial z^2} - f(\bar{u} - \bar{u}_g) = 0. \tag{14.2.24}$$

The derivation of the above equations is similar to that of (14.2.17), except that the K-theory parameterization is adopted instead of the bulk parameterization. Introducing a new complex variable, $u + iv$, (14.2.23), and (14.2.24) can be combined into a single equation,

$$K_m \frac{\partial^2 (\bar{u} + i\bar{v})}{\partial z^2} - if(\bar{u} + i\bar{v}) = -if(\bar{u}_g + i\bar{v}_g). \tag{14.2.25}$$

The solution of (14.2.25) subjected to the no-slip boundary conditions at the ground, $\bar{u} = \bar{v} = 0$ at $z = 0$, and approaching geostrophic wind speeds far from the ground, i.e. $\bar{u} \to \bar{u}_g$ and $\bar{v} \to \bar{v}_g$ as $z \to \infty$ is

$$\bar{u} = \bar{u}_g (1 - e^{-\gamma z} \cos \gamma z); \ \bar{v} = \bar{u}_g e^{-\gamma z} \sin \gamma z, \tag{14.2.26}$$

where $\gamma = (f/2K_m)^{1/2}$. The above solution is sketched in Fig. 14.4. The wind veers (i.e. turns clockwise) and increases with height to be slightly over the geostrophic value, and then reaches to be nearly the geostrophic value at $z = \pi/\gamma$, which may also be defined as the Ekman layer depth. The spiral wind profile is known as *Ekman spiral*.

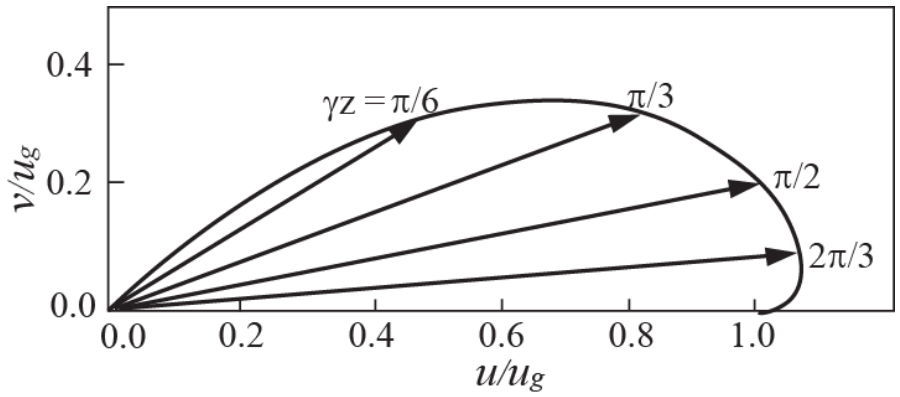

Fig. 14.4: A sketch of the wind vectors of the Ekman spiral (14.2.26). The arrows show the wind vectors at non-dimensional height $\gamma z = \pi/6, \pi/3, \pi/2, 2\pi/3$, where γ is defined in (14.2.26). (Adapted after Batchelor 1967)

c. Turbulent kinetic energy closure scheme

The first-order closure schemes, such as K-theory parameterization, may be improved by predicting one of the subgrid-scale variables, the turbulent kinetic energy (TKE) per unit mass $\left[e = (\overline{u'^2} + \overline{v'^2} + \overline{w'^2})/2 \right]$, while the other subgrid scale turbulent flux terms are diagnosed and related to both the TKE and the grid-scale mean values.

The prognostic prediction of TKE in the parameterization scheme is referred to as the *TKE* or *one-and-a-half-order closure*.

When the Reynolds number of a laminar flow increases, it may break down into a turbulent flow. A turbulent flow is characterized by high randomness, nonlinearity, diffusivity, vorticity, and dissipation. The breakdown is often associated with instability, such as shear instability or buoyant (static) instability. Shear and buoyancy are the two major sources of the production of TKE, which may be denoted as *S* and *B*, respectively. Once the turbulence is generated and fully developed into a steady state in terms of averaged flow properties, then the instability is no longer required to sustain the turbulent flow. In order to reach steady state turbulence (statistically), certain mechanisms are required to remove and redistribute TKE. These mechanisms are often attributed to the dissipation (*D*) due to turbulent eddy viscosity and molecular viscosity, and the transport and redistribution (*Tr*) due to advection and pressure forces. Thus, the time evolution of TKE can be written as

$$De/Dt = S + B + Tr - D\,. \tag{14.2.27}$$

To derive the mathematical form of the TKE equation, we first substitute $u = \bar{u} + u'$, $v = \bar{v} + v'$, $w = \bar{w} + w'$, $p = \bar{p} + p' = p_o + p_1 + p'$, $\theta = \bar{\theta} + \theta' = \theta_o + \theta_1 + \theta'$, $\rho = \bar{\rho} + \rho' = \rho_o + \rho_1 + \rho'$ into (13.5.6)-(13.5.8) with *f* neglected, to obtain,

$$\frac{D(\bar{u}+u')}{Dt} = -\frac{1}{\rho_o}\frac{\partial(\bar{p}+p')}{\partial x} + \nu\nabla^2(\bar{u}+u')\,, \tag{14.2.28}$$

$$\frac{D(\bar{v}+v')}{Dt} = -\frac{1}{\rho_o}\frac{\partial(\bar{p}+p')}{\partial y} + \nu\nabla^2(\bar{v}+v')\,, \tag{14.2.29}$$

$$\frac{D(\bar{w}+w')}{Dt} = -\frac{1}{\rho_o}\frac{\partial(p_1+p')}{\partial z} - \frac{g}{\rho_o}(\rho_1+\rho') + \nu\nabla^2(\bar{w}+w')\,. \tag{14.2.30}$$

Unlike in Section 14.1, in deriving the above equation, we have used the partition of $\bar{p}$ and $\bar{\rho}$ into hydrostatic (p_o and ρ_o − large scale) and nonhydrostatic (p_1 and ρ_1 − mesoscale) parts, neglected ρ_1 and ρ' relative to ρ_o except in the buoyancy (associated with the gravity) term, and assumed an anelastic fluid. Now, multiplying (14.2.28)-(14.2.30) by u', v', w', respectively, and then taking the Reynolds averaging over a grid volume lead to the *TKE equation*,

$$\frac{\partial \overline{e}}{\partial t} = -\overline{\boldsymbol{V}} \cdot \nabla \overline{e} - \overline{\boldsymbol{V}' \cdot \nabla e} - \left(\frac{1}{\rho_o}\right)\left[(\overline{u'p'})_x + (\overline{v'p'})_y + (\overline{w'p'})_z\right] - \left(\frac{g}{\rho_o}\right)\overline{\rho' w'}$$

1 2 3 4

$$-\left[\left(\overline{u'u'}\,\overline{u}_x + \overline{u'v'}\,\overline{u}_y + \overline{u'w'}\,\overline{u}_z\right) + \left(\overline{u'v'}\,\overline{v}_x + \overline{v'v'}\,\overline{v}_y + \overline{v'w'}\,\overline{v}_z\right)\right. \quad ,$$

5

$$\left. + \left(\overline{u'w'}\,\overline{w}_x + \overline{v'w'}\,\overline{w}_y + \overline{w'w'}\,\overline{w}_z\right)\right] + \nu\nabla^2\overline{e} - \nu\left(\overline{u'^2_x} + \overline{v'^2_y} + \overline{w'^2_z}\right)$$

6 7

(14.2.31)

The left-hand side of (14.2.31) represents the local rate of change of the TKE.

Term 1: advection of $\overline{e}$ by the grid-volume averaged velocity
Term 2: grid-volume average of the advection of TKE by the subgrid-scale perturbation velocity.
Term 3: change in TKE by advection through the boundaries of the grid volume (Term 3 is difficult to measure and is thus often ignored in the closure problem.)
Term 4: buoyancy production of the TKE
Term 5: shear production of the TKE
Term 6: diffusion of turbulence by molecular diffusion
Term 7: sink of TKE by molecular diffusion.
(In mesoscale modeling, Terms 6 and 7 are often ignored.)

d. Higher-order closure schemes

In fact, subgrid-scale perturbations such as u', v', w', and θ', can be predicted by subtracting the resolved flow equations from the full equations, similar to the derivation of TKE equation. The proposed method will generate new unknown variables involving triple correlation of the perturbations, which must be represented by the mean variables and quadratic perturbation terms, in order to close the system mathematically.

One can go further by deriving the prediction equations for the third moments and close the system on higher-order correlation terms (Mellor and Yamada 1974), commonly referred to as the *higher-order closures*.

The higher-order closure schemes are capable of representing a well-mixed layer structure. Figure 14.5 shows a comparison of numerically simulated virtual potential temperature profiles in the boundary layer for Day 33 of the Wangara experiment by using a TKE closure scheme and a third-order closure scheme, and the observational data. The TKE closure scheme (Fig. 14.5a) is capable of capturing the observed major features (Fig. 14.5c) compared to the third-order closure scheme (Fig. 14.5b). The higher-order closure schemes are computationally expensive and do not necessarily make a significant improvement in accurately parameterizing the PBL compared to lower-order closure schemes, such as TKE.

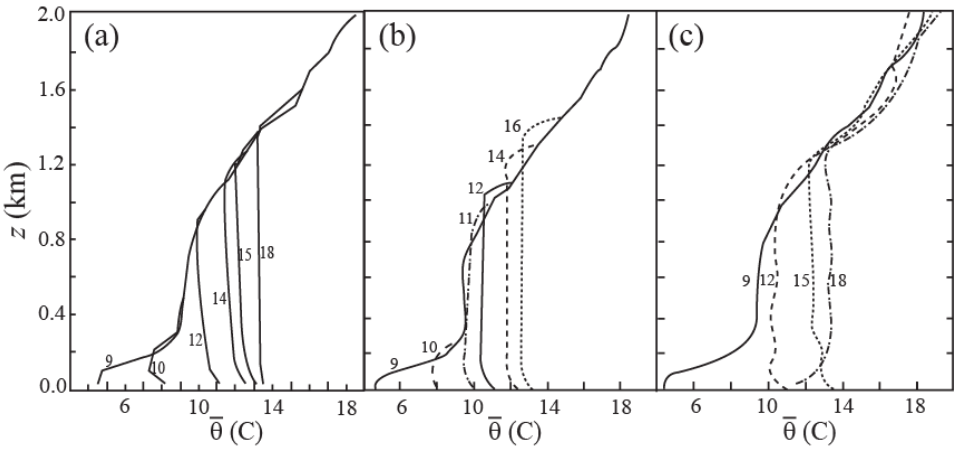

Fig. 14.5: Comparison of predictions of the virtual potential temperature profile using (a) TKE closure scheme (Adapted after Sun and Chang 1986) and (b) third-order closure scheme (Adapted after André et al. 1978) for Day 33 of the Wangara experiment against (c) observational data (Adapted after André et al. 1978). The local times are denoted by the numbers adjacent to the curves.